A Methodology to Derive Wind Tunnel Wall Corrections from RANS Simulations

Jean-Luc Hantrais-Gervois* and Jean-François Piat**
*Onera – The French Aerospace Lab
F-92190, Meudon
FRANCE

Jean-Luc.Hantrais-Gervois@onera.fr

**Onera – The French Aerospace Lab
F-73500, Modane
FRANCE

ABSTRACT

This paper presents a methodology to estimate the wind tunnel wall interference with RANS simulations. The method involves a pairing process between confined and aerodynamically equivalent free air simulations that is carried out through automatic optimisation. Wall corrections are derived for a major industrial wind tunnel (ONERA S2MA wind tunnel located in Modane). In order to model the porous test section walls in the RANS simulations, the characteristics of the walls were measured with a specific experiment. On the whole, in the linear aerodynamic domain, the RANS corrections are similar to the current correction strategy but require a higher CPU cost. The benefit appears in non-linear regimes (high lift or high Mach number).

1.0 BACKGROUND OF WALL INTERFERENCE

1.1 Primary corrections and residual corrections

Each aircraft undergoes intensive wind tunnel test campaigns before the maiden flights. Because of the wind tunnel walls, the in tunnel flow deviates from free air aerodynamics (see Figure 1). The wind tunnel operator transposes the rough aerodynamic measurements to equivalent free air aerodynamic data. The purpose of the wind tunnel wall corrections consists in:

- Defining the closest fictive free air physical state corresponding to the aerodynamic state measured in the confined environment. These twin states are not identical, but they present similar features (average pressure level and shock position, see Figure 1). This is the purpose of the **primary corrections** (ΔM, $\Delta \alpha$, $\Delta \beta$) to the main aerodynamic parameters. These corrections are an average global correction. When large interferences are experienced, no equivalent free air flow can be defined and the flow cannot be corrected. This can occur when the model is too large for the wind tunnel (the obstruction should not exceed 1% for transonic tests) or when too high Mach numbers are tested (the tunnel can even be shocked).

- Accounting for the residual deviations to the average equivalent free air flow. These corrections correspond to local deviations of the aerodynamic field (for example see Figure 2). The integration of these local effects consists in the **residual corrections** to the forces and moments ($\Delta \vec{F}$, $\Delta \vec{M}$).
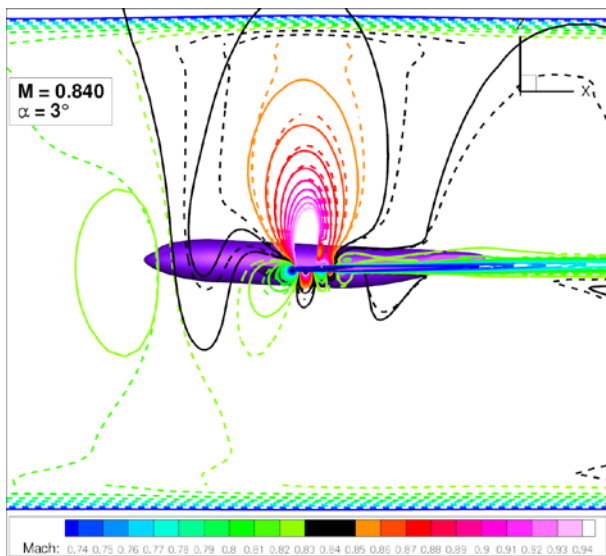
Figure 1: Comparison of iso-Mach number lines in free-air (solid lines) and confined environments (dashed lines).
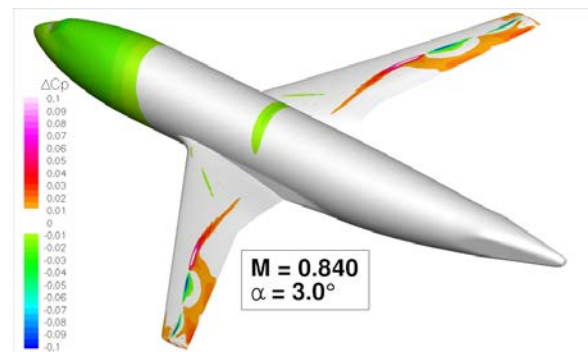

Figure 2: Cp deviations between free-air and confined environments.

1.2   Computational Fluid Dynamics (CFD) for the evaluation of wall interference

1.2.1   State of the art

The state of the art of the wall interference estimation is well presented in an exhaustive AGARD publication [1]. Depending on the wind tunnel, the estimation methods can be empirical (based on comparisons with reference wind tunnels either large or with a guided test section), analytical (formulations based upon the potential flow model resorting for instance to wall pressure signatures and Green functions), computational (up to Euler simulations as in the AEDC [2]).

Since that period, RANS CFD has entered the wind tunnel. Several teams have included parts of the wind tunnel in their numerical simulations to model more precisely the flow and improve their numerical – experimental comparisons (see for example [3]). The effects of the wind tunnel walls are also gaining interest in the case of profile aerodynamics for the wind turbines [4] or for the unsteady phenomenon such as the dynamic stall [5]. An advanced use of RANS CFD to complement the wind tunnel measurements in transonic wind tunnels is developed at TsAGI [6] and JAXA [7]. These approaches resort to a detailed modelling of the porous wind tunnel test sections. In both cases CFD enhances the knowledge of the model aerodynamics within the wind tunnel. Nevertheless, CFD is not used to define wall corrections to be applied within the whole wind tunnel correction system to derive corrected datasets.

At ONERA, in the large industrial facilities in Modane, the wall interference is estimated with the linear potential flow code DXV [9] (with some experimental contributions). This method is very efficient and proved accurate among the numerous wind tunnel tests carried out in Modane. Nevertheless, the linear potential flow assumption is not adequate for high transonic Mach numbers, large model obstructions or high angles of attack near the maximum lift. The use of RANS CFD to enhance this correction procedure has been approached in [10] for the two main transonic facilities in Modane (S1MA and S2MA).

1.2.2   Scope of this communication

This paper presents a correction methodology based on RANS simulations that encompasses in a single method both the corrections to the reference state and the corrections to forces and moments. The principle is to match automatically simulations of the model in the wind tunnel with free air simulations. The corrections being derived by differences between paired simulations, the RANS CFD is only required to predict increments. The use of these numerical corrections within the complete wind tunnel correction procedure will be detailed. This paper is a revised version of [11].

The methodology is applied to a major industrial facility (S2MA wind tunnel located in Modane). The tunnel is a transonic pressurised tunnel with perforated walls that can be sealed to achieve a guided test section. A detailed focus of an experimental characterisation of the porous walls will be given. A third chapter will present the numerical modelisations of the wind tunnel.

Finally, a validation of the confined simulations will be presented prior discussing the values of corrections obtained by the RANS simulations in comparison with the correction process in use at ONERA.

2.0   RANS METHODOLOGY TO COMPUTE WALL INTERFERENCE

2.1   Wall correction process in use at ONERA

To produce the results of the tests, the raw measurements of the balance weighting the model are converted into aerodynamic coefficients through several modifications:

1   measurement of balance signals (electric signals);

2   conversion of these signals into Newton and Newton times meters;

3   derivation of the aerodynamic conditions in the wind tunnel;

4   reduction of forces and moments to get aerodynamic coefficients;

5   estimation of the aerodynamic interferences (walls, sting);

6   interpolation of all the results to produce polars at round values of Mach numbers, if necessary (thanks to the Mach number stability in the tunnel considered in this paper, this step is not applied).
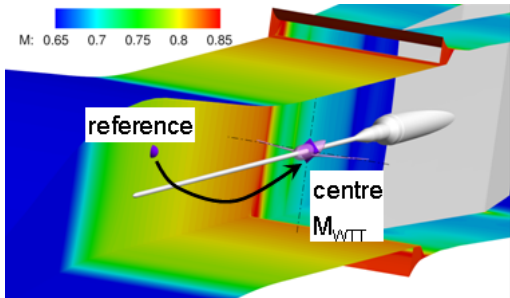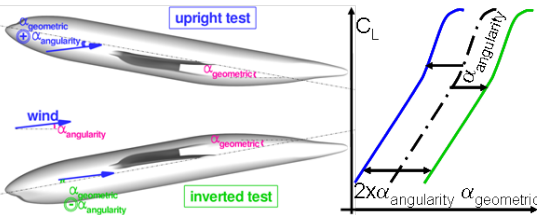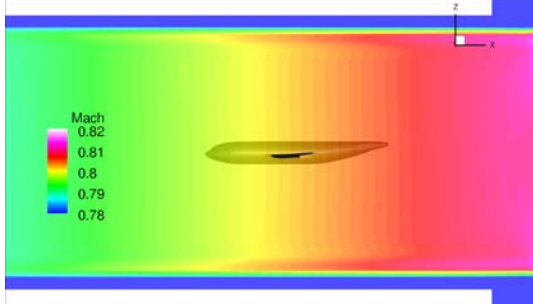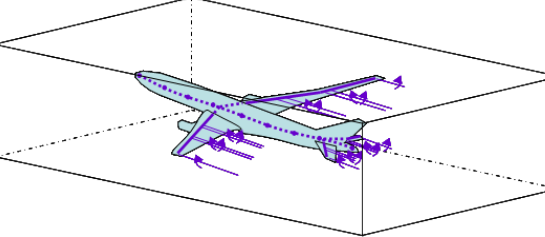
Looking into the details of the 3rd and 5th points (see Table 1), the correction process is decomposed into several contributions estimated either through experimental calibrations or through basic aerodynamic simulations. For a wind tunnel operator, the wall interference term refers to the estimation of the confined flow interference for the model (part of the 5th step). The other steps are considered as wind tunnel calibrations. All the steps are connected with the wall interference topic as treated in this communication.

For the ONERA wind tunnels, the wall corrections are assessed using an analytic method called DXV based on the linearised potential equation [9]. The main interest of this method is that the mathematical formulation relies on the addition of the perturbations. Thus, the wall influence is directly known from a unique simulation of the flow field in the wind tunnel with the installed model. The model is simulated by singularities (sources, sinks and doublets for the fuselage, horseshoe vortices for the wings). For guided test sections, a slipping boundary condition is modelled and the wall effect is simply the effect of the infinite series of model "images" through the four walls. For porous test sections the walls are modelled with a velocity through the perforated wall proportional to the pressure drop through the wall (between plenum and test section). An adequate choice of the location of the correction to the angle of attack (at 75% of the aerodynamic mean chord, see [12]) enables to derive corrections at iso-lift.

Typically, under the best conditions (adequate balance, model and aerodynamic conditions), a good

performance wind tunnel test aims at reaching an accuracy of ±1 10⁻³ in Mach number, ±0.01° in angle of attack, ±1 10⁻⁴ in drag, ±1 10⁻³ in lift and ±1 10⁻³ in pitching moment. We see that the levels of corrections are well above these accuracies. Nevertheless, this does not impact the quality of the test because the corrections are well handled.

Table 1: Wall correction procedure in use in the ONERA wind tunnels.

Type of correction	Explanation	Typical values Guided test section (porous test section)
Determination of the uncorrected Mach number M_WTT. The tunnel reference tap is located upstream of the model and it provides an indication of a tunnel Mach number at the tunnel centre (unperturbed by the model). This Mach number is only a convention that does not reflect a real aerodynamic state for the model. The link between the reference tap and the tunnel centre is made thanks to empty tunnel calibrations carried out over the Mach number range.	*Empty tunnel calibration with a centreline probe (the model is represented to show its position in the test section).*	$M_{WTT} = M_{reference} + \Delta M_{calibration}$ $\Delta M_{calibration}$ depends on the reference tap position.
Determination of the uncorrected angle of attack α_WTT. The geometric inclination of the model is measured through a goniometer. But each wind tunnel features a flow angularity that is inherited from the history of the air circuit and the tunnel design. This angularity is obtained by comparing lift polars obtained in upright and inverted model position	*Principle of the upright and inverted tests to determine the flow angularity.*	$\Delta\alpha_{angularity} \approx 0.1°$ (0.1°), mostly independent on the test conditions.
Determination of a buoyancy correction on drag $\Delta C_{D\ buoyancy}$. Each wind tunnel presents an evolution of the Mach number from the nose to the tail of the models. The Mach number evolution is measured during the empty wind tunnel calibration and the gradient (buoyancy) is applied to the surfaces of each model. The correction accounts for the boundary layer growth and the wall divergence (evolution of the tunnel area).	*Empty tunnel Mach number gradient (solid walls). The model is represented to show its position within this gradient.*	Highly dependent on the tunnel, the Mach number and the model. For solid wall tunnels without wall divergence compensating the boundary layer growth, about 15 dc can be achieved. In porous tunnels or guided tunnels with wall divergence about ±2 dc can be achieved.
Determination of the wall corrections (ΔM, Δα) and ($\Delta\vec{F}$, $\Delta\vec{M}$). This step accounts for the interaction between the model and the walls. At ONERA these corrections related to the walls are achieved through CFD (linear potential). The walls are modelled parallel and without boundary layer.	*Principle of the linear potential simulations to estimate the wall interference.*	$\Delta M \approx$ from 0 to 10 10⁻³ (less than 2 10⁻³), highly dependent on M. $\Delta\alpha \approx$ from 0.0° to 0.3° (less than 0.1°) and highly dependent on lift. $\Delta C_D \approx 5\ 10^{-4}$ (5 10⁻⁴). $\Delta C_m \approx 2\ 10^{-3}$ (2 10⁻³).

2.2 RANS wind tunnel correction methodology

2.2.1 RANS correction procedure

Contrary to the potential flow approach, a single RANS simulation does not provide directly the additive effects of the walls on a model. Using RANS simulations that are non-linear and thus non-additive in nature, implies to come back to the definition of the corrections. The corrections aiming at relating a confined flow field to an equivalent free stream flow field, pairs of RANS simulations need to be computed: one free air simulation of the model paired with one in-tunnel simulation. These effects might be determined in the presence of the sting line or without.

The interest of this method relies on its exhaustiveness. If the confined simulation reflects correctly the confined flow physics, the comparison of the flow fields of the pair of computations provides directly the primary and residual corrections:

- Primary corrections (ΔM, $\Delta \alpha$): the free stream Mach number corresponding to the confined flow field is known without resorting to a fictive uncorrected confined Mach number. Both the empty tunnel effects and wall interference are accounted for. The angle of attack correction contains the flow angularity and the wall interference. In this communication, sideslip will not be considered as both S2MA and the models are symmetric.

- Residual corrections ($\Delta \vec{F}$, $\Delta \vec{M}$): the corrections to the forces and moments are self-sufficient, and especially, the buoyancy is embedded in the pair of simulations.

This method supposes to be able to match pairs of simulations and to exploit the pairs to derive the corrections. So as to correct a wind tunnel test, a matrix of aerodynamic conditions (M, α) needs to be assessed to cover the aerodynamic domain.

This simple approach is appealing, but it has two major drawbacks: i) it can't be connected with actual correction procedure and ii) it supposes a perfect modelling of the flow physics of the wind tunnel. Thus, in order to be able to validate separately the tunnel calibration and the corrections, the experimental process must be mimicked numerically. Thus, empty tunnel simulations have to be computed. These simulations can be carried out once and for all for one wind tunnel as it has no connection with any model to be tested in the test section.

Finally, 3 different simulations must be obtained for a set of correction at (M_∞, α_∞) that can be embedded in the current wind tunnel correction procedure:

1. empty wind tunnel simulation to be able to define the fictive confined Mach number, the flow angularity and the buoyancy correction;

2. free air simulation at (M_∞, α_∞);

3. in-tunnel simulation with adapted (M_{WTT}, α_{WTT}) to match the aerodynamic of the free air simulation.

2.2.2 Pairing process

The free-air and the confined simulations are said to be paired when the flow fields around the wing are similar. In this study, the criterion of similarity is based on the pressure field at the skin. The pressure is converted into the isentropic Mach number in order to work with figures without dimensions that can easily be compared for different Mach numbers and especially different stagnation pressures. As the in-tunnel pressure field is distorted on the wing, an exact match cannot exist. Thus the isentropic Mach number on each cell is compared between the free-air and the confined simulations. We then sum the deltas (squared) for each cell (with a weighting by the cell area) and divide by area covered by the considered cells. Taking the square root of this figure corresponds to the root mean square error of the Mach number fields and it is

used in this study as the similarity factor (see Figure 3). Two paired fields achieve a minimal similarity factor.

In this study, the similarity factor is computed on the suction side where the relevant transonic flow features arise. The pressure side might be added for low lift coefficients.
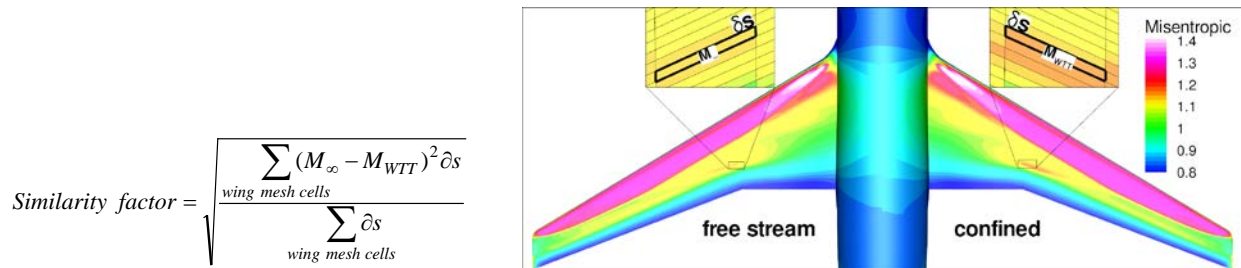

$$Similarity\ factor = \sqrt{\frac{\sum\limits_{wing\ mesh\ cells}(M_\infty - M_{WTT})^2 \partial s}{\sum\limits_{wing\ mesh\ cells}\partial s}}$$

Figure 3: Definition of the similarity factor between the free air and the confined simulations.

In practice, for a given aerodynamic condition in the wind tunnel (M_{WTT}, α_{WTT}), the equivalent aerodynamic condition in free air must be searched by adjusting the (M_∞, α_∞) couple until the similarity factor is deemed satisfying. The process can also be inversed when a precise (M_∞, α_∞) is the main interest. In that case, the confined conditions are adjusted. An example of optimisation process is sketched in Figure 4 where the gradient based optimization strategy developed by Vanderplaats [13] is used within the optimization software DAKOTA [14]. A loop in python language [15] enables to feed the optimizer with evaluations of (M_{WTT}, α_{WTT}) couples. About 25 simulations free-air simulations are carried out to match a given in-tunnel simulation.
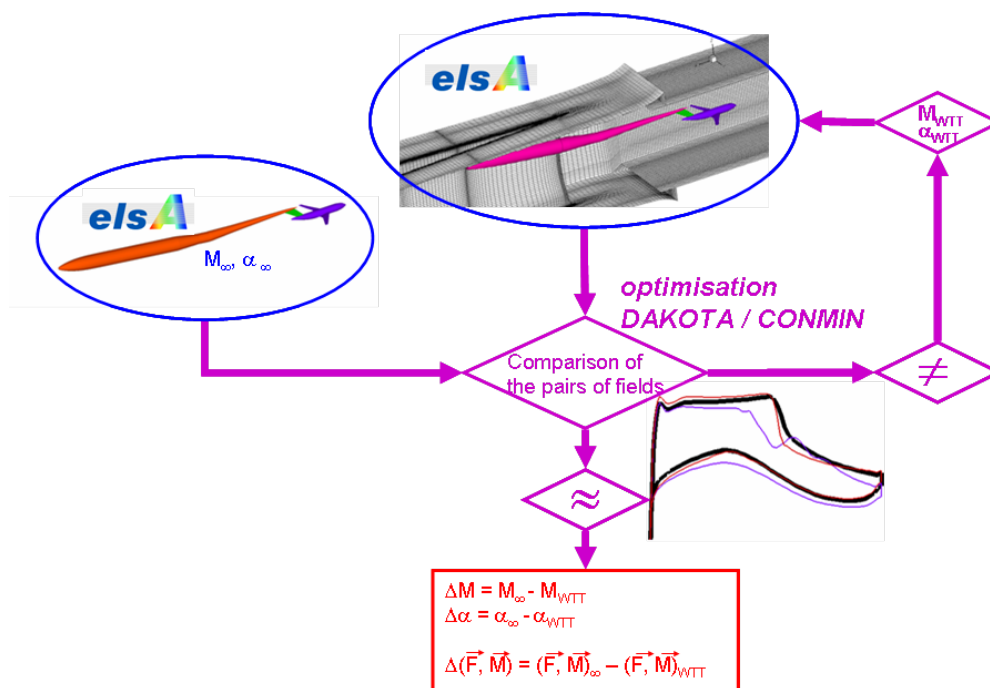

Figure 4: Pairing procedure by optimisation.

2.2.3   Empty tunnel simulations

To separate the empty tunnel effects from the pure wall interference, empty tunnel simulations can be carried out. The wind tunnel geometry from the settling chamber needs modelling in the RANS simulations (see Figure 5). The Mach number evolution with the tunnel contraction and boundary layer development is thus modelled, together with the flow orientation. These simulations deliver numerical equivalents for quantities used in actual correction process:

- Simulating a range of Mach numbers and stagnation pressures (once and for all) allows establishing the numerical calibration between the reference sensor on the wall and the centre of the tunnel. Thus, $M_{WTT\ CFD}$ can be determined in the same fashion as in the experiments.

- The integration of the Mach number gradient over the model provides the numerical buoyancy drag ($\Delta C_{D\ buoyancy\ CFD}$). This gradient can be removed from the Cp discrepancy between the free stream and the confined simulations to separate the model – wall interference effects from buoyancy (see Figure 6). This can be directly compared the linear potential flow simulations.

- In these simulations, the numerical flow angularity can also be determined ($\alpha_{angularity\ CFD}$). Nevertheless, this quantity can't be directly compared to the experimental one because the flow simulation does not account for the flow history in the wind tunnel air circuit. In the simulations, the flow in the settling chamber is supposed strictly horizontal and homogeneous.
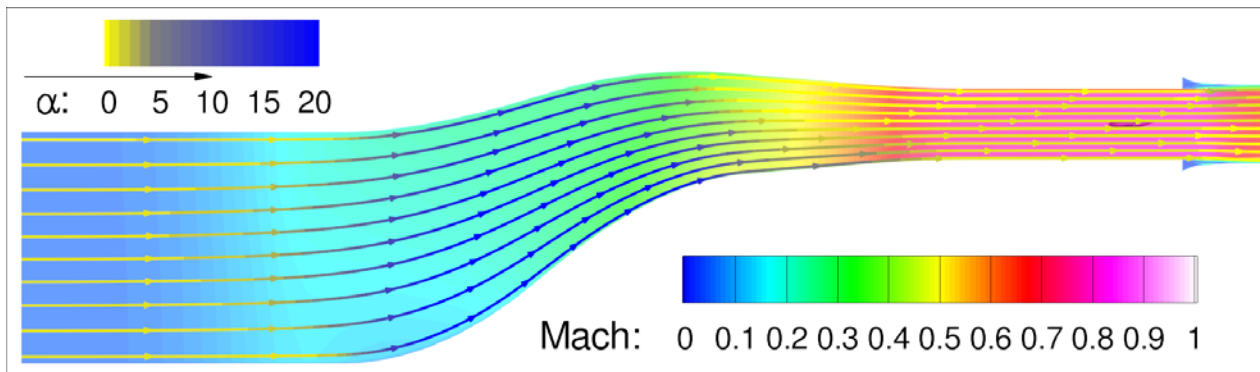

Figure 5: Empty tunnel flow simulations taking into account the flow accelerations and orientation (the model is shown in the test section, but it is not included in the computations).
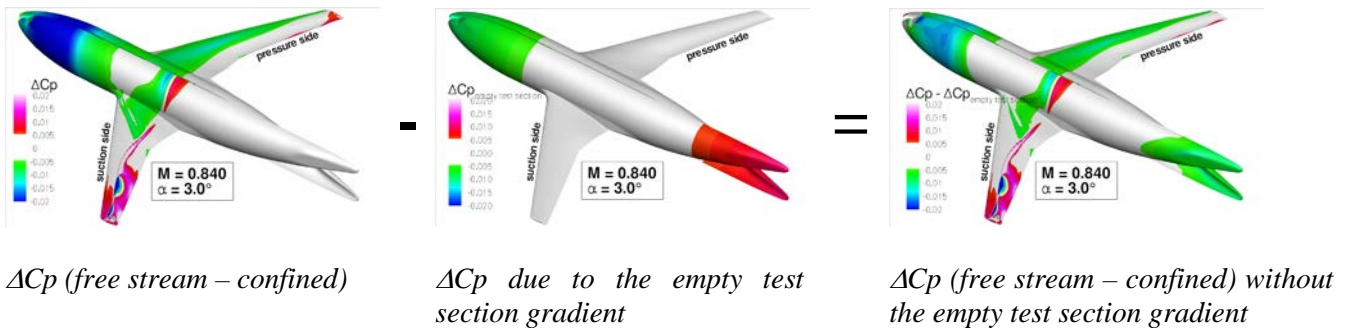

ΔCp (free stream – confined)   *ΔCp due to the empty test section gradient*   *ΔCp (free stream – confined) without the empty test section gradient*

Figure 6: Distinction between the buoyancy and the other wall effects on the model (guided test section).

2.2.4   Deriving the RANS wall corrections

When pairs of simulations are obtained, it is possible to compare the aerodynamic conditions (M, α) and the aerodynamic coefficients to derive the primary and residual corrections.

For the primary corrections, a direct comparison of the conventional Mach number of the confined simulation to the Mach number of the free stream simulation gives ΔM. For the correction in angle of attack, the numerical empty test section angularity is combined with the geometric angle of attack of the model in the wind tunnel to define the uncorrected angle of attack. A direct comparison with the free stream angle of attack provides $\Delta\alpha$.

Once the free stream Mach number is established, the corresponding free stream dynamic pressure is used to remove the dimension from the aerodynamic coefficients for both the free stream and the confined forces and moments. In this communication, the forces and moments are expressed in the body axis to avoid any conflict between the coefficients and the angle of attack. Thus, we will look at the normal force (CN), the axial force (CA) and the pitching moment (Cm).

The corrections to forces and moments are deduced from the differences between the integrated forces over the model in free-stream and confined environments. These corrections originate from local deviations of the flow field between the confined and the free air environments (see Figure 6). In this RANS approach, the corrections include both the effect of empty tunnel buoyancy and the other interference effects. So as to separate the effects for comparison with the experimental procedure, the buoyancy can be estimated using the empty tunnel gradients.

The current correction procedure with potential flow simulations is such that the confined states correspond to the free air states at the same lift (here, $\Delta CN = 0$). With the RANS simulations, two paired simulations exhibit a different lift coefficient (see Figure 7). Thus, for a direct comparison with the linear potential flow corrections, the RANS corrections presented in this paper have been interpolated to be derived at fixed normal coefficient. This choice is neutral to correct polars, but it removes the link between the pressure on the model and the associated lift.
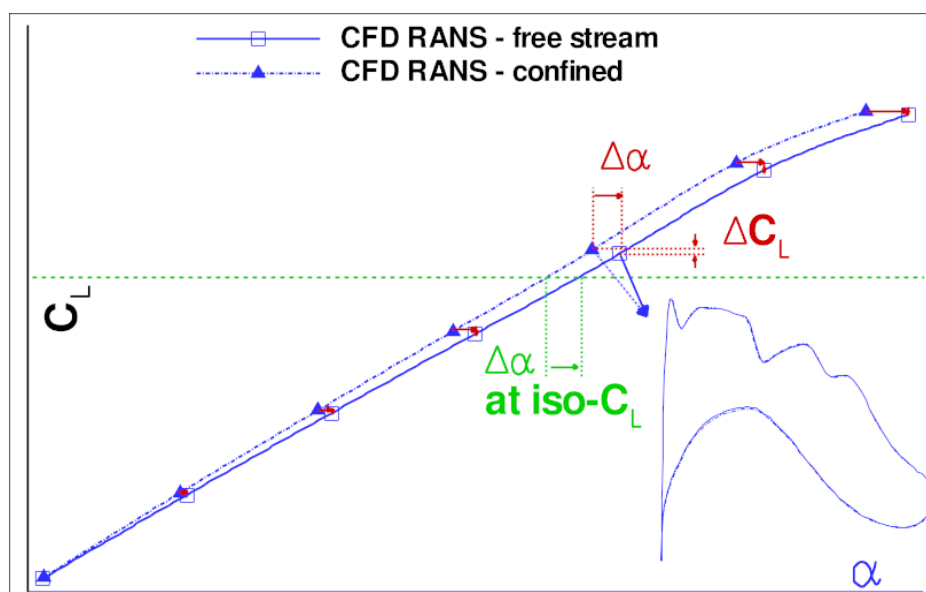

Figure 7: RANS corrections at iso-lift.

3.0 S2MA WIND TUNNEL AND POROUS WALLS

3.1 Generic features

Among the ONERA facilities in Modane-Avrieux, the S2MA wind tunnel has been chosen for this numerical application because of its intensive use for industrial purposes (see Figure 8). The facility can be operated for transonic and supersonic regimes with a possibility to vary the stagnation pressure from 0.2 up to 2.5 bars. It presents a rectangular test section by 1.75 m width and 1.77 m high (test section area 3.1 m^2).
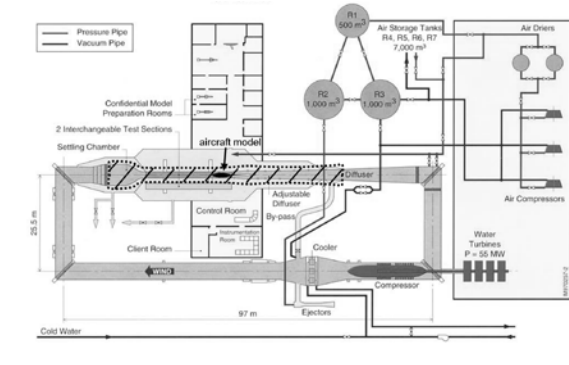

Figure 8: S2MA air circuit (the hatched zone represents the portions modelled in this study).
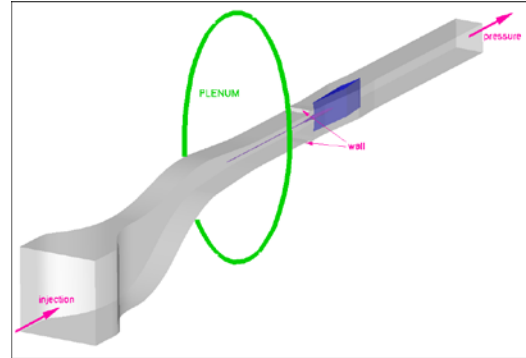

Figure 9: Numerical model of the S2MA wind tunnel.

3.2 Description of the porous walls

Wall porosity is used in transonic wind tunnels to limit the wall interference and to avoid blockage. In S2MA, the porosity consists in holes drilled in the upper and bottom walls with an inclination (see Figure 10 and Figure 11). The inclination tends to favour the movement of air from the test section to the plenum. On the plenum side of the porous plates, a grid was used to adapt the effective porosity. Nowadays, this grid is fixed and the porosity is 5.2% for each top and bottom wall (or 2.6% for the entire test section).

Porosity evolves longitudinally along the test section (see Figure 12 to Figure 15). In the first third of the test section (upstream) porosity is progressive. The last two thirds are porous but not completely periodic because of the beams sustaining mechanically the porous (some holes are more closed than others).

The setting of the walls is set at null inclination. Nevertheless, the Mach number gradient is about zero since the flow outside of the test section compensates the growth of the boundary layer. When a guided test section behaviour is needed, the holes are sealed, and a Mach number gradient is present.
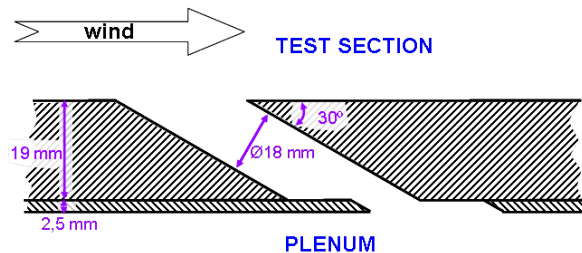

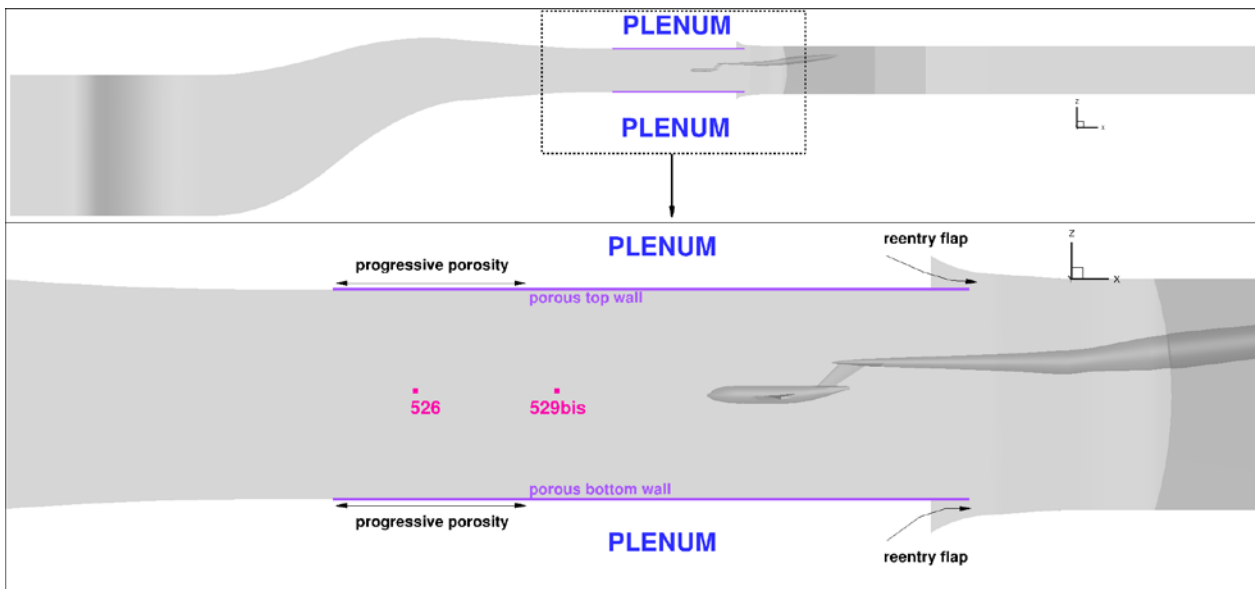**Figure 10: Porous wall of the S2MA test section.**

Figure 11: Hole layout in S2MA.

Figure 12: General arrangement of the S2MA test section and the porous walls.

Figure 13: Progressive porosity.

Figure 14: Top wall (with a pressure rail).

Figure 15: Re-entry flaps.

3.3   Measurements of the S2MA wall porosity

3.3.1   Experimental set up

The objective of the tests is to measure the cross flow characteristic of the portion of the porous wall. It consists in measuring the relation between the flow velocity through the porous wall $w = m/\rho_0 S$ and the pressure coefficient in the plenum $C_P = (P_c - P_0)/Q_0$. We then seek the function $w/V_0 = f(C_P)$. Where ρ_0, P_0, Q_0, V_0 are the density, static pressure, kinetic pressure and velocity of the wind tunnel flow.

The test set up is presented schematically in Figure 16. A can was installed in the plenum on the top porous wall, upright the test section centre (Figure 17). Its height was 0.4 m and it covered an area **S** equal to 0.112 m², including about thirty holes. The can was connected through a flexible tube to a high pressure supply or to a vacuum supply, located outside the wind tunnel. The high pressure came from a big sphere with an adjustable pressure, up to 64 bars. The low pressure was obtained with the help of an ejector supplied by the high pressure from the sphere.

The air mass flow **m** going through the can and the porous wall could be adjusted by means of control valves, from 0.03 kg.s⁻¹ to 1 kg.s⁻¹, and was measured by a sonic flowmeter (pressure) or by a venturi

(vacuum). At the beginning of the test, the can had been isolated and the sonic flowmeter and the venturi had been connected on the same circuit. A very good agreement was observed between the two mass flow measurements.

The pressure inside the can was measured by 4 transducers and the mean value **Pc** was calculated.

In addition, in order to examine the local flow disturbances on the test section side of the porous wall, a boundary layer rake and a static pressure rail were installed on the top wall (Figure 16 and Figure 14). The rake was located at about 0.2 m downstream from the tested wall portion. The rail had a length equal to 0.7 m and was located at about 0.15 m on the side of the tested wall portion.

The experiments were performed in the empty test section (no model) at:

- Mach number M = 0.70, 0.80, 0.85 and 0.90;

- stagnation pressure Pi = 1.0, 1.5 and 2 bars;

- about twenty mass flow values for each (M, Pi) condition, including inflow (from the plenum to the test section) and outflow (from the test section to the plenum).
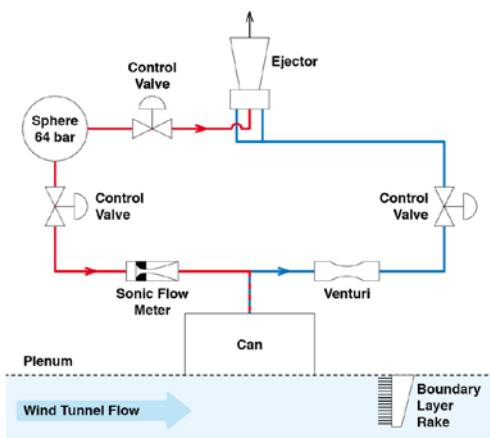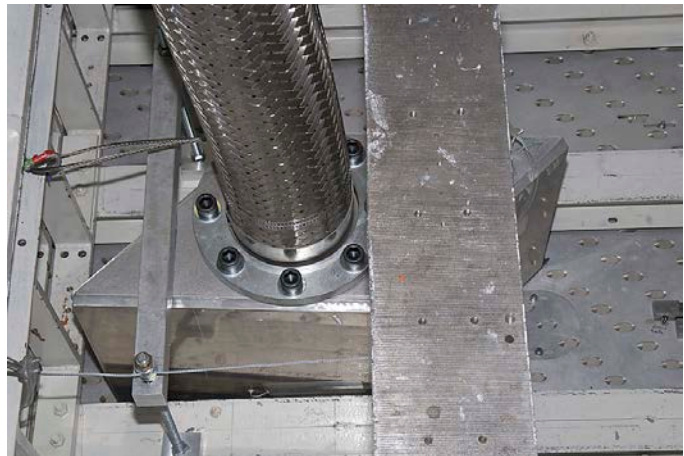

Figure 16: General set up.

Figure 17: Set up of the can in the plenum.

3.3.2 Experimental results and discussion

The cross flow correlation $w/V_0 = f(C_P)$, measured at M = 0.80 and Pi = 1 bar, is shown in Figure 18. The following comments can be given:

- repeatability of measurements between two runs, performed at the beginning and at the end of the test, is very good;

- as expected, the vertical velocity is much higher for the outflow than for the inflow since the holes are inclined in the wind direction;

- the mass flow m = 0 is obtained for Cp = 0.065. Since during tests in S2MA the pressure coefficient of the plenum is about equal to 0.040 and change in Cp at the bottom and top walls induced by the model are typically limited to ± 0.020, the difference in Cp through the porous walls range from 0.020 and 0.060, being wholly in outflow. As a conclusion the S2MA test section runs nearly always

in outflow;

- over the Cp range of usual tests (0.02 to 0.06), the graph in Figure 18 looks relatively well linear. The use of a constant porosity coefficient, whatever the Cp level, in the flow simulations when modelling the porous walls, is so justified;

- it is to be noted that the porosity coefficient derived from Figure 18 is equal to only about 2/3 of the coefficient used in the linear potential flow code and which was determined empirically. In fact the relevant vertical velocity w for this latter code is the one measured at the outer boundary of the wall boundary layer [21]. The longitudinal change in the boundary layer displacement thickness $\frac{d\partial 1}{dx}$ amplifies the vertical velocity at the wall. Recent boundary layer measurements in the S2MA test section showed that this amplification explained roughly the 1/3 lacking.

The change in cross flow correlation in terms of Pi, measured at M = 0.80, is shown in Figure 19. Deviations are low, significant only at Pi = 2 bars in outflow and in the beginning of inflow.

The change in cross flow correlation with Mach number is shown in Figure 20 (measured at Pi = 1 bar). Deviations are about zero in inflow but notable in outflow; so between M = 0.70 and 0.90, over the usual test Cp range, the porosity (slope) is reduced by 1/3.

The velocity distribution into the boundary layer measured by the rake for a large range of mass flow is presented in Figure 21. As expected the boundary layer gets thinner in outflow and grows in inflow. The displacement thickness $\partial 1$, which is equal to 11 mm for the mass flow m = 0, reaches 6 mm and 23 mm for the extreme mass flow.
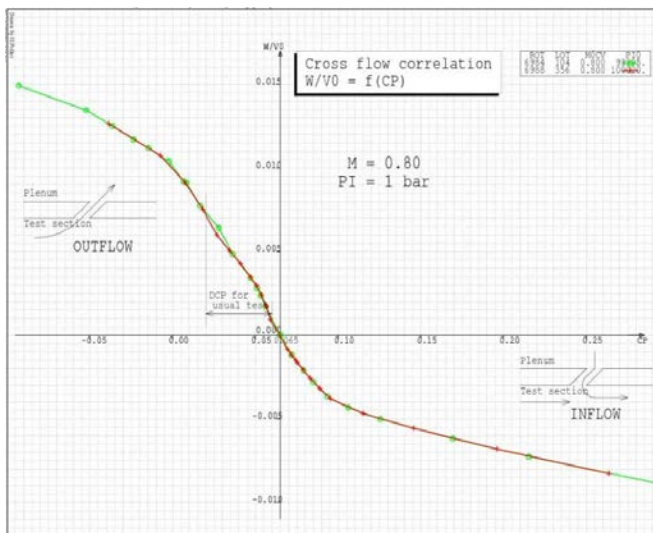

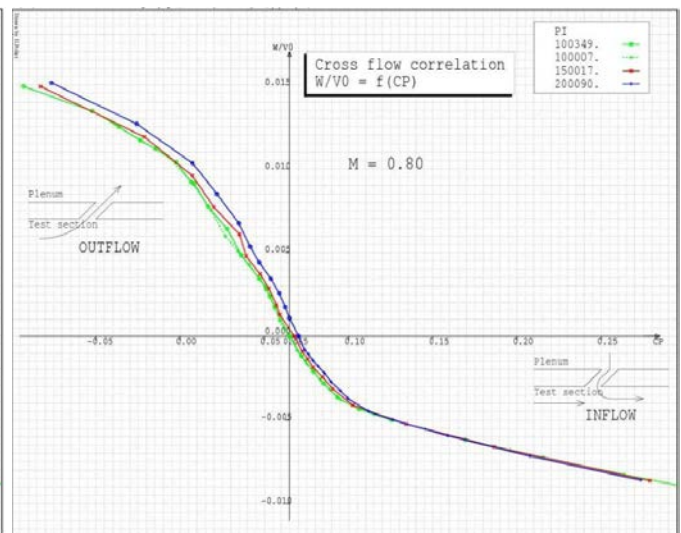**Figure 18: Repeatability of the cross flow correlation.**

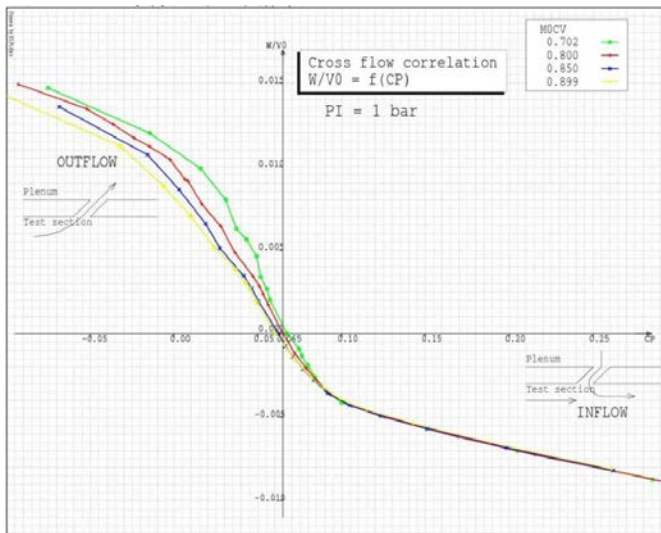**Figure 19: Stagnation pressure effect.**
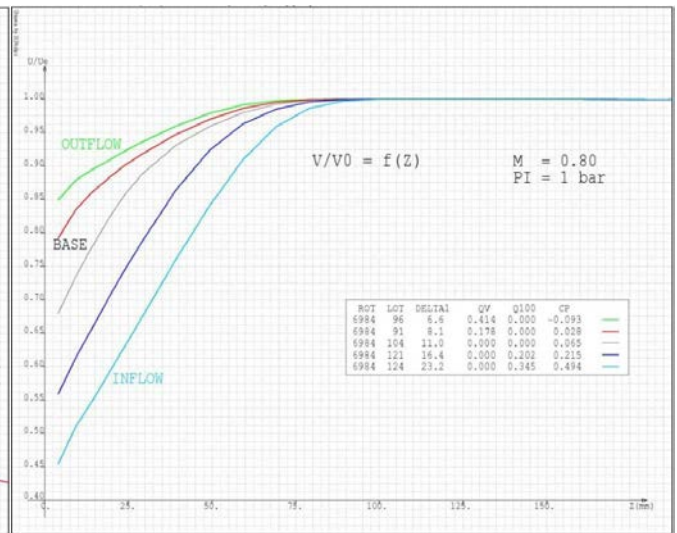
Figure 20: Mach number effect.

Figure 21: Velocity distribution into the boundary layer.

4.0   NUMERICAL MODELS FOR THE CFD SIMULATIONS

4.1   S2MA wind tunnel

This study builds upon a former study dedicated to the validation of the numerical tools to model the confined flows in wind tunnels (see [16], [17]).

As for the purpose of the wall interference, we need to represent several important factors such as the growth of the boundary layers in the test section (progressive contraction of the apparent tunnel section). Thus, the wind tunnel has been modelled from the settling chambers to the diffuser (see Figure 9).

From a numerical point of view, apart from walls, the boundary conditions consist in the inlet (settling chamber) and the outlet (part of the diffuser). Only half of the CAD could be meshed with 3.1 million nodes (structured mesh), thanks to the left-right symmetry. For the wind tunnel walls, the y+ varies between 0.7 and 2.0 depending on the stagnation pressure in the wind tunnel.

4.2   Model and sting line

The S2MA wind tunnel was computed with its reference model (A310 research wing body model on a fin sting, see the experimental set-up in Figure 22). This model cruises at Mach number 0.80 and the blockage ratio in the S2MA test section is 0.8%.

The structured mesh of the model features 3.5 million nodes and the sting line features 0.9 million nodes (see Figure 23). An additional cartesian bloc (1.4 million nodes) around the model ensures correct interpolations between the small cells around the A310 research model and the S2MA relatively large cells. The complete configuration installed in the S2MA test section features about 9 million nodes.

Due to the geometric complexity of the elements present in any wind tunnel (sector, sting, blade, model) the Chimera technique has been used (see [18], [19]). The technique consists in overlapping grids. The meshing process is eased because more simple elements are meshed. The assembly of the grids is ensured through
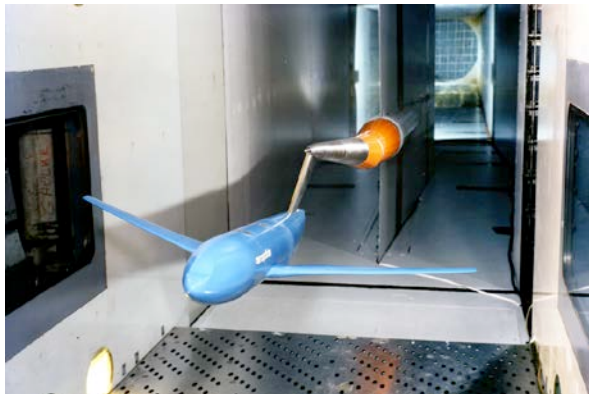
high order interpolations.

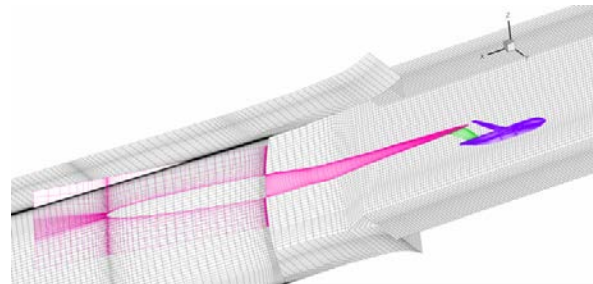**Figure 22: A310 model installed in the S2MA wind tunnel.**

Figure 23: Mesh of the A310 research model in the S2MA test section.

4.3 Numerical software

The computations resort to RANS modelling computed with the elsA software [20]. The software solves the equations in a finite volume formulation (cell-centred). For this study, a LU implicit scheme has been used together with a second order central difference for the spatial discretisation of the mean flow (Jameson scheme with second and fourth order dissipation terms). As for the turbulent quantities, a first order central discretisation is used. The time scheme is the first order backward-Euler. The local time stepping and multigrid techniques are applied to speed up the convergence process. The turbulence model is the one equation Spalart-Allmaras.

4.4 Boundary condition formulation in the RANS software

The experimental porous boundary condition has been implemented in the elsA aerodynamic software. The formulation consists in a modification to the wall boundary condition. The non slip boundary condition formulation is modified to allow an added momentum perpendicular to the wall. In each wall cell, the momentum depends on the local pressure.

For solid walls, the communication with the plenum was simply blocked and setting the static pressure at the diffuser directly sets the Mach number in the test section. With porous walls the test section aerodynamic conditions are now determined from three different places of exchange with the fluid outside of the computation domain (each involving a specific pressure parameter):

- settling chamber (stagnation pressure);
- diffuser (static pressure);
- plenum (stagnation pressure).

Several attempts have been tried to determine an adequate plenum pressure automatically adjusted from the diffuser pressure, but the results were not stable. Thus, the experimental pressures have been directly used for both the diffuser and the plenum pressure. Another formulation should be attempted to free the simulations from the dependence on the experimental values.

Another aspect must be taken care of. As the porous walls see mainly outflow, a balance must be achieved between the plenum and the test section. This balance is established through the re-entry flaps at the end of

the test section, upstream of the sector (see Figure 12). In order to model this balance and conserve the global mass in the wind tunnel, an iterative process is carried out:

- porous simulation with an average inflow at the re-entry flaps;

- integration of the outflow over the porous walls at the end of the simulation;

- new porous simulation with an inflow at the re-entry flaps corresponding to previous porous wall outflow.

Rapidly, the mass fluxes reach stable values (two coupling steps are sufficient).

4.4.1   Validation of the porous formulation

A validation has been carried out for the empty tunnel at various Mach numbers. For this paper, as corrections will be derived only for Pi = 1.5 bar and M = 0.80, only the porous characteristics at these conditions are used.

A preliminary validation consists in verifying that the boundary condition is used in the range of the measurements. In Figure 24, the velocity at the porous wall is represented, together with the velocity in the re-entry flaps. In the empty test section (see Figure 24 a), the velocity evolves rapidly from the most upstream part of the porous wall to reach about 0.5 m.s^{-1} over most of the porous wall. Then, locally, the velocity rises at the re-entry flaps to reach about 1 or 2 m.s^{-1}. In the computations with the model at cruise (see Figure 24 b) the velocities are more contrasted. The velocities can reach locally 1 m.s^{-1} and some inflow through the porous walls can occur in the vicinity of the model (at low velocity).

These velocities are well in the range of the linear region found in the porosity measurements. The inflow through the re-entry flaps corresponds to about 10 to 15 m.s^{-1}.
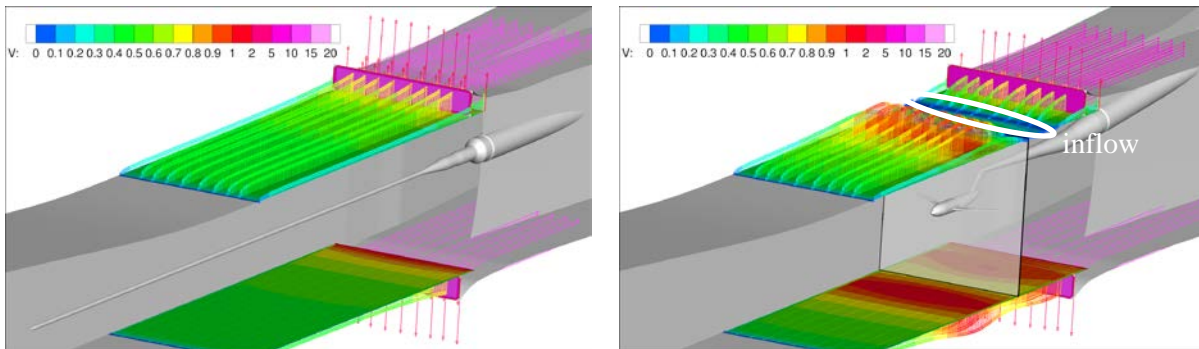
a) empty test section   *b) with the model in cruise conditions*

Figure 24: Examples of velocities through the porous walls at M = 0.800.

5.0   ASSESSMENT OF THE CONFINED FLOW SIMULATIONS

5.1   Wall signatures in the empty tunnel

The wall signatures obtained with CFD are compared to the experimental ones in Figure 25. A good match is achieved all along the wind tunnel, from the convergent to the diffuser, for both the guided and the porous test sections. The various Mach numbers tested exhibit satisfying results. In the vicinity of the model where all the wall interference resides, the diminution of the Mach number gradient from guided to porous is well

simulated by RANS CFD.

When the simulations are carried out for several test conditions, it is possible to determine the numerical calibration of the empty wind tunnel. In Figure 26, several relations are presented for the RANS simulations and for the experiments (both guided and porous walls):

- The relation between the tunnel reference pressure tap and the centre of the tunnel is in green. This relation will enable to define the uncorrected Mach number for the confined simulations with the model.

- The relation between the Mach number in the centre of the tunnel and the pressure at the diffuser is in black. This relation shows the link between the locus where the boundary condition is applied (diffuser) in the simulation and the achieved Mach number at the tunnel centre.

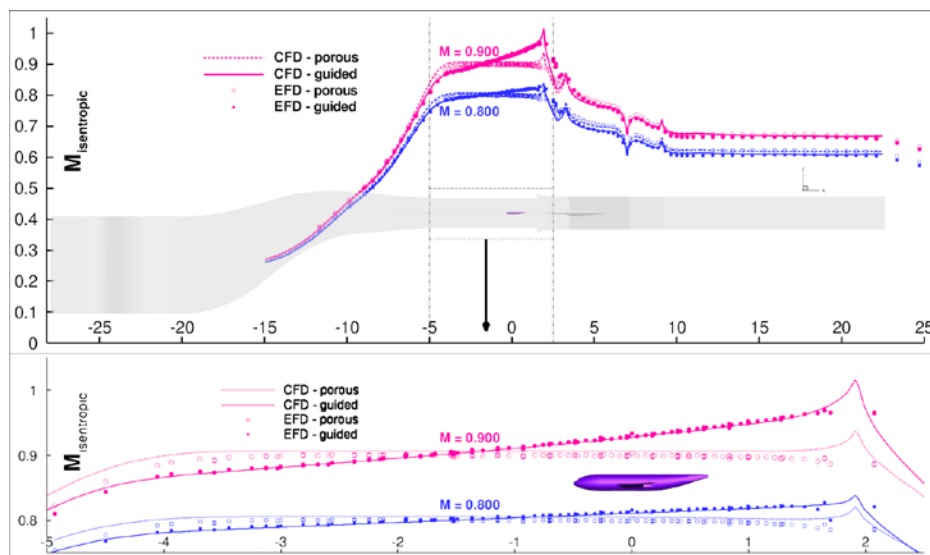Both relations compare well with the experiments, for both the guided and the porous test sections.

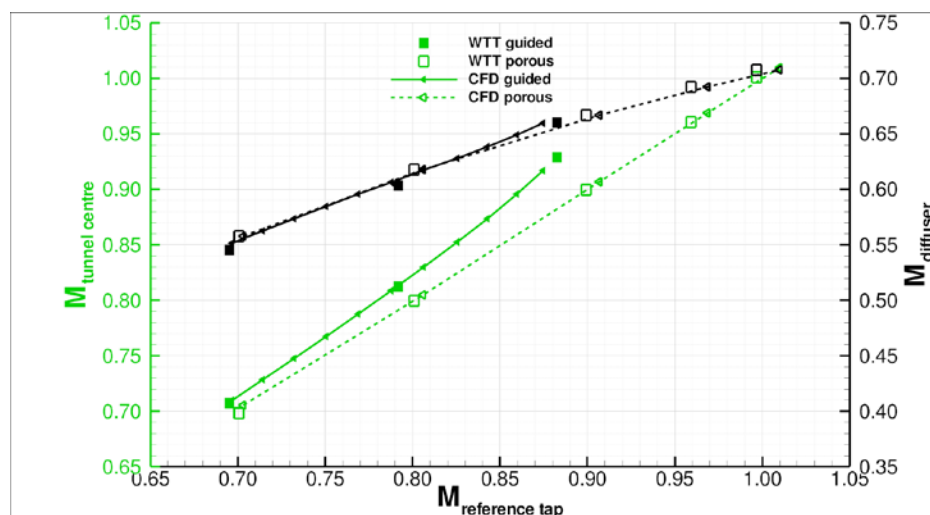**Figure 25: Empty tunnel wall signatures for the guided and the porous test sections.**

Figure 26: Numerical and experimental empty tunnel calibrations (guided and porous walls).

5.2 Wall signatures with the model in S2MA

Based on the good validations achieved for the empty tunnel simulations the validation is now carried out on the tunnel with the model and its sting line. The validation resorts to the comparison of wall signatures on several rows of pressure taps between CFD and EFD (Experimental Fluid Dynamics).

The comparison is carried out by subtracting the pressure without model (empty wind tunnel) from the pressure with model (see Figure 27). This enables comparing with the potential flow code that does not account for empty tunnel gradients. This operation also removes the empty test section Mach number gradient and the Mach number is constant upstream of the model. Near the model, the top and bottom signatures separate because of the effects of lift and we can see a larger effect in the guided test section than in the porous one. Across the model (nose to tail), a gradient is noticeable and it continues downstream of the model.

The general trends are correctly predicted by both the RANS simulations and the linear potential code. Especially on the guided test section, a very good agreement between all the methods is achieved. For the porous test section, a too large Mach number gradient across the model is present in the RANS simulations, whereas the potential flow simulations predict very well the pressure signatures in both conditions.

Globally, the RANS results are in a good agreement with the experiments and we can thus proceed to the analysis of the corrections.
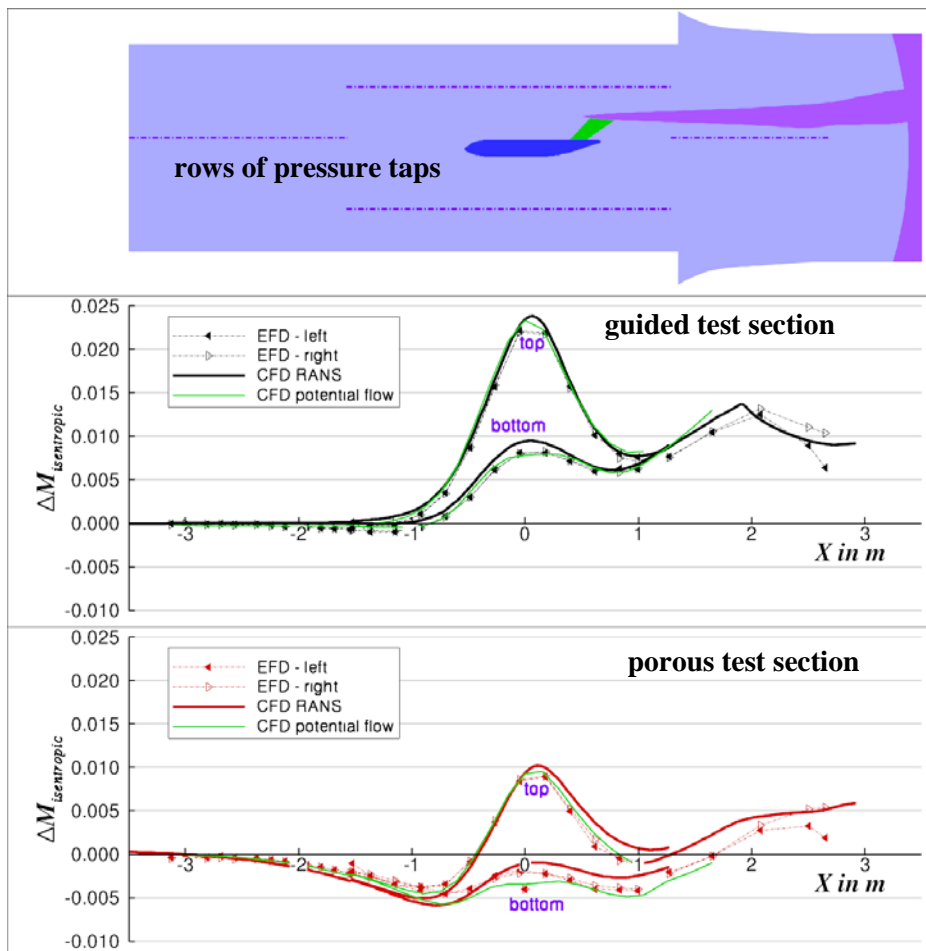

Figure 27: Wall signatures in S2MA at cruise (M = 0.80, CL = 0.50).

6.0   DISCUSSION ON THE WALL CORRECTIONS

Two sets of computations are presented in this paper.

The first set of computations aims at validating the RANS correction process against the linear potential flow method. In order to do so, we have represented the guided test section (well defined wall boundary treatment) and the model without the sting line (to remove the junction between the model and the sting that is difficult to model with singularities). Mach number regimes from linear to non-linear have been explored (from 0.700 to 0.840).

The second set of computations includes the sting line and the porous walls. They aim at testing the RANS correction procedure on a concrete applied case (at M = 0.800 only).

6.1   Primary corrections (ΔM, Δα)

The primary corrections are presented in Figure 28. For the Mach number correction (red lines), a good general agreement is found between the potential flow simulations and the RANS simulations. In the guided test section, the corrections range from 0.004 to 0.012 from low Mach number to high transonic Mach number. A gradient in Mach number correction is shown in the RANS simulations between the zero lift to the high lift for the transonic cases (evolution in Mach number correction by about 0.002). The discrepancy between the methods lies within ±0.001 in Mach number correction. For the porous test section, the average correction in Mach number is nearly null, but the RANS simulations exhibit a ±0.002 variability. The correction at low lift exhibits a reverse trend but it is deemed unreliable because of the low quality of the pairing for this point.

For the angle of attack correction, a good agreement is achieved for both the porous and the guided test sections. The reduction of the slope of the correction with lift in the porous case is well predicted, and the minor impact of the Mach number effect in the guided test section is confirmed. Nevertheless, the RANS corrections exhibit a tendency to move from a linear behaviour at high lift. This trend increases with the Mach number.
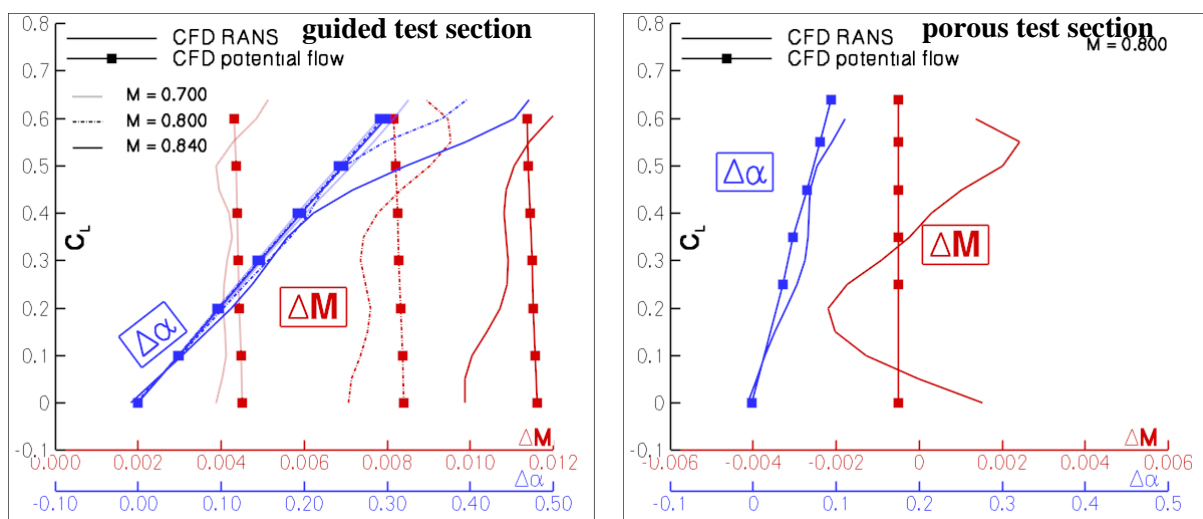

Figure 28: Primary corrections in S2MA.

6.2 Residual corrections ($\Delta\vec{F}$, $\Delta\vec{M}$)

The pitching moment correction is shown in Figure 29 (top). For the guided test section, the corrections obtained by RANS and potential flow models are in good agreement at low lift (discrepancy in correction lower than 1 10^{-3}). For high lift coefficients the RANS corrections deviate rapidly from the linear potential flow corrections. In the porous test section, the corrections are similar in trend but with a deviation by about 2 10^{-3}. This discrepancy originates from the rear fuselage with the fin sting. In these areas, the RANS CFD provides detailed flow patterns whereas the linear potential CFD has difficulties in modelling the geometry.

The corrections in axial coefficient are presented in Figure 29 (bottom) and a good match between the approaches is evidenced. The EFD corrections contain both the linear potential corrections and the experimental buoyancy for a direct comparison to the RANS corrections. In the guided test section, an excellent match is achieved at M = 0.700 (discrepancies lower than ±1 dc). When Mach number increases, the RANS corrections exhibit local deviations from the average CA correction along the lift polar (discrepancy in correction ±2 dc for an average correction by about 20 dc). As for the porous test section, a large discrepancy between the RANS simulations and the EFD corrections can be noted (about 8 dc). Again, the discrepancy originates from the rear fuselage (fin sting model plus fuselage contraction).
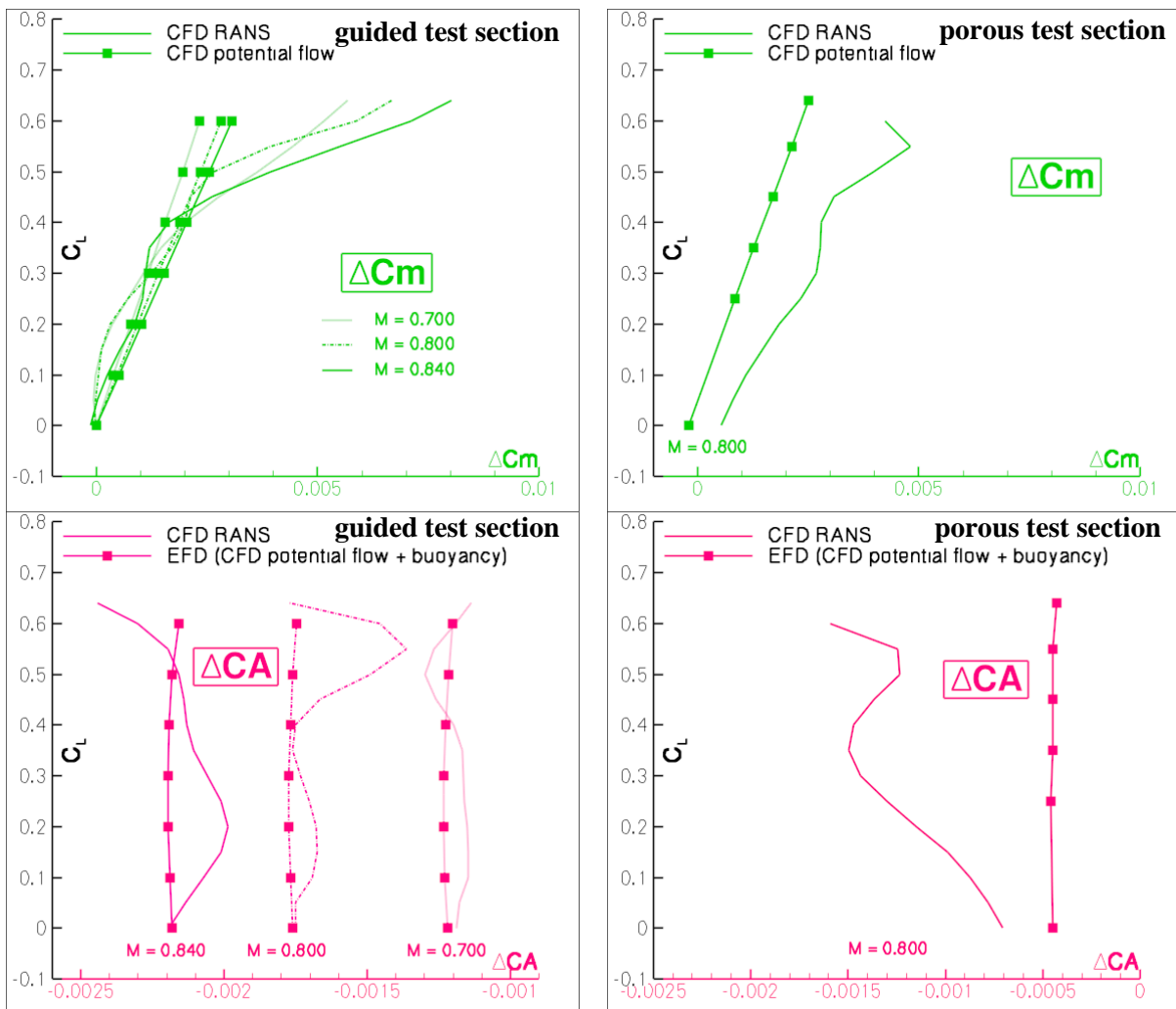

Figure 29: Residual corrections (pitching moment on top and axial coefficient in the bottom).

So as to go further in the analysis of the RANS correction procedure in comparison with the linear potential approach used currently at ONERA, it is also possible to compare the interference in axial force without the buoyancy (see Figure 30 a). This is directly what the linear potential code predicts. At this scale, we can see that only about 2 dc correction remains. But for this correction, a difference by about 2 dc can be experienced between the RANS and the linear potential code.

To investigate this difference, this correction is split between its components for the fuselage and for the wing (see Figure 30 b and c). Even if the pressure discrepancies between the confined flow and free air were especially visible on the wing, they are very local and thus, the corrections on the wing are marginal (less than ±1 dc). The correction on the fuselage is the most important one. The same progression with Mach number is present in the RANS simulation and in the linear potential flow corrections. Nevertheless the RANS corrections exhibit an influence of the lift that increases with Mach number when the linear potential flow corrections are constant in lift. We can see a close match at the low Mach number where the flow is indeed linear and a discrepancy by about ±1 dc at high Mach number when non-linearities arise.

If we compare the CA correction in Figure 30 (without buoyancy) to the correction in the porous test section in Figure 29 (that contains only few buoyancy), we may have the false impression that the correction is larger in the porous test section. If the magnitude of the correction is larger, this is because of the presence of the sting in that case. When looking at comparable settings (wall interference in the presence of the sting for example), the porous and the guided test sections produce about the same interference (this is not shown in this paper).
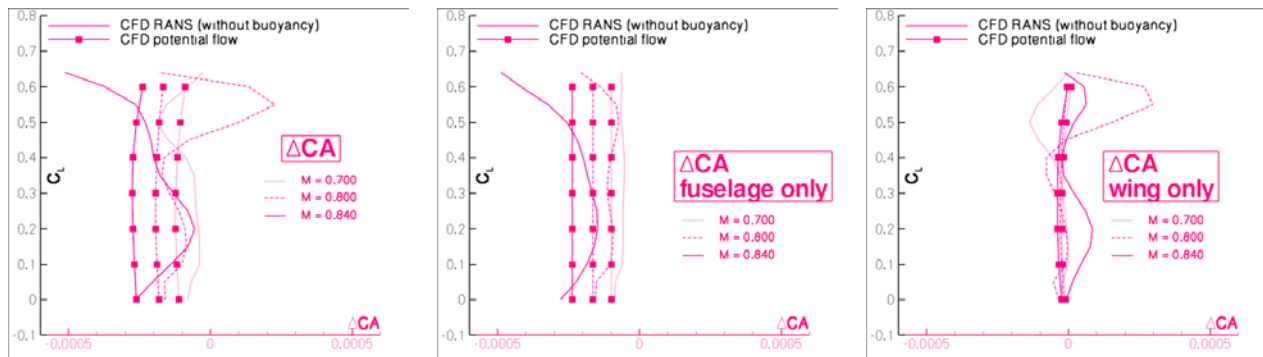
a) Correction for the whole model
b) Correction for the fuselage
c) Correction for the wing

Figure 30: Breakdown of the axial coefficient correction without buoyancy (guided test section).

7.0 CONCLUSIONS AND PERSPECTIVES

This paper describes in details a methodology to estimate the wind tunnel wall interference with RANS simulations. We have taken care of the experimental aspects to define a concrete process that can be embedded in current test data process. The current ONERA method relying on fast linear potential flow simulations, we have focused on the benefit that could be gained from the modelling of non-linearities with high fidelity RANS simulations (requiring more CPU time). The paper presents both methodological developments and applied simulations on a transonic ONERA wind tunnel in Modane (pressurised S2MA tunnel with both guided and porous walls).

The RANS simulations need to model the physics of the confined flows including boundary layer development over the tunnel walls, accelerated and decelerated flows in the convergent and the diffuser,

corner flows at the tunnel wall junctions and aerodynamic interference between the model and the confined environment. A specific attention has been devoted to the modelling of the S2MA porous walls thanks to a measurement campaign focusing on the average porosity characteristics of this wind tunnel. Good validations with wall signatures have been achieved on the empty tunnel and on the tunnel with the model. Some complementary modelling activities on the porous test section should be carried out.

Thanks to the use of automatic optimisation to obtain equivalent simulations in free air and in the wind tunnel, RANS wall corrections could be established for many test conditions (Mach number and angle of attack) and test set up (porous or guided, with or without model support). The comparison of the RANS corrections with the current correction procedure has enabled to draw several conclusions. In terms of CPU cost, the potential flow simulation requires only seconds whereas the RANS procedure requires several days and can't be operated in real time during a test. As for accuracy, both correction procedures predict similar correction levels for the aerodynamic conditions (primary corrections) as well as for the aerodynamic coefficients (residual corrections). The differences arise at high lift or high Mach number when the non-linearities increase. In these regimes, the RANS corrections show a non-linear behaviour whereas the potential flow corrections remain intrinsically linear.

The procedure developed to compute the corrections being principally an automated means of finding pairs of similar flows, it can handle any interference effect such as mounting effects, for instance. Finally, we should focus on only the two meaningful configurations of interest: model with its sting line in the wind tunnel and model in free stream. Thus, the intermediate steps with the model with its sting in free stream allowing computing wall interference in the presence of the sting and sting interference without walls can be avoided to tackle directly the global and coupled wall and support interference.

8.0   ACKNOWLEDGEMENTS

9.0   REFERENCES

[1] Ashill P.R., Binion T., Cooper K.R., Crites R., Everhart J.L., Ewald B.F., Hackett J., Holst H., Krynytzky A.J., Malmuth N.D., Mokry M., Newman P.A., Sickles W.L., Steilne F.W.J., Taylor C.R., Taylor N.J., Voss R., Wedemeyer E.H.: Wind Tunnel Wall Corrections, *AGARD Advisory Group for Aerospace Research and Development*, AGARD-AG-336, 1998.

[2] Kraft E.M., Ritter A., Laster M.L.: Advances at EADC in Treating Transonic Wind Tunnel Wall Interference. *15th Congress of the International Council of the Aeronautical Sciences*, Vol. 2, pp. 748-769, 1986.

[3] Schuh M. J., Garcia J. A., Carter M. B., Deere K. A., Stremel P. M. and Tompkins, D.: NASA Environmentally Responsible Aviation Hybrid Wing Body Flow-Through Nacelle Wind Tunnel CFD (Invited), *54th AIAA Aerospace Sciences Meeting*, San Diego, California, USA, January 2016. doi: 10.2514/6.2016-0263.

[4] Kuhn T., Altmikus A., Balaresque N. and Lippert M.: Numerical Replication and Improvement of Wind Tunnel Tests for Design and Off-Design Operating Points of Wind Turbine Airfoils, *33rd AIAA Applied Aerodynamics Conference*, Dallas, Texas, USA, June 2015. doi: 10.2514/6.2015-2577.

[5] Duraisamy K., Mc Croskey W. J. and Baeder J. D.: Analysis of Wind Tunnel Wall Interference Effects on Subsonic Unsteady Airfoil Flows, *Journal of Aircraft*, vol. 44, no. 5, pp. 1683-1690, September 2007. doi: 10.2514/1.28143.

[6] Bosnyakov S., Kursakov I., Lysenkov A., Matyash S., Mikhailov S., Vlasenko V., Quest J.: Computational Tools for Supporting the Testing of Civil Aircraft Configurations in Wind Tunnels. *Progress in Aerospace Sciences*, No. 44, pp 67-120, 2008. doi: 10.1016/j.paerosci.2007.10.003.

[7] Hashimoto A. and Kohzai M.: Wall Interference Analysis by Whole Wind Tunnel CFD, *Integration 2012*, JAXA Chofu Aerospace Center, Tokyo, Japan, October 2012.

[8] Kohzai M., Sudani N., Yamamoto K., Ueno M., Hashimoto A.: Experimental and Numerical Studies of Support Interference in the JAXA 2m x 2m Transonic Wind Tunnel. *27th AIAA Aerodynamic Measurement Technology and Ground Testing Conference*, 2010.

[9] Vaucheret X.: Recent Calculation Progress on Wall Interferences in Industrial Wind Tunnels. *La Recherche Aérospatiale*, No. 3, pp 45-47, 1988.

[10] Hantrais-Gervois J.-L., Mouton S. and Piat J.-F., RANS simulations to compute wind tunnel wall corrections, *47th International Symposium of Applied Aerodynamics*, Paris, France, 2012.

[11] Hantrais-Gervois J.-L. and Piat J.-F.: A Methodology to Derive Wind Tunnel Wall Corrections from RANS Simulations, *Integration 2012*, JAXA Chofu Aerospace Center, Tokyo, Japan, October 2012.

[12] Pistolesi, E.: Considerations respecting the mutual influence of system of airfoils. *Collected lectures of the principal meeting of the Lilienthal society*, Berlin, 1937.

[13] Vanderplaats G.N.: CONMIN – A FORTRAN Program for Constrained Function Minimization. User's Manual. NASA TMX 62282, 1973.

[14] The DAKOTA Project, Large-Scale Engineering Optimization and Uncertainty Analysis, http://www.cs.sandia.gov/DAKOTA

[15] Python Programming Language, http://www.python.org

[16] Hantrais-Gervois J.-L., Cartiéri A., Mouton S., Piat J.-F.: Empty Wind Tunnel Flow Field Computations. *AAAF, 44ᵗʰ Applied Aerodynamics Symposium*, Nantes, 2009.

[17] Hantrais-Gervois J.-L., Cartiéri A., Mouton S., Piat J.-F.: Empty wind tunnel flow field computations. *Int. J. Engineering Systems Modelling and Simulation*, Vol. 2, No. 1/2, 2010. doi: 10.1504/IJESMS.2010.03187.

[18] Benek J.A., Steger J.L., Dougherty F.C.: A Flexible Grid Embedding Technique with Application to the Euler Equations. *AIAA Aerospace Science Meeting & Exhibit*, 1983.

[19] Benoit C., Jeanfaivre G., Canonne E.: Synthesis of ONERA Chimera Method Developed in the Frame of CHANCE Program. *31ˢᵗ European Rotorcraft Forum*, Florence, 2005.

[20] Cambier L., Heib S., Plot S.: The Onera elsA CFD Software: Input from Research and Feedback from Industry, *Mechanics & Industry*, Num.3, Vol. 14, April 2013

[21] Crites R. and Rueger M.: Modeling the ventilated wind tunnel wall. *30ᵗʰ AIAA Aerospace Sciences Meeting and Exhibit*, Reno, Nevada, 1992.